catalysts

MDPI

Article

Cu/O Frustrated Lewis Pairs on Cu Doped CeO_2(111) for Acetylene Hydrogenation: A First-Principles Study

Shulan Zhou [1,2,*], Qiang Wan [3] and Sen Lin [3,*]

[1] School of Chemistry and Chemical Engineering, Shandong University of Technology, Zibo 255049, China
[2] Department of Material Science and Engineering, Jingdezhen Ceramic Institute, Jingdezhen 333403, China
[3] State Key Laboratory of Photocatalysis on Energy and Environment, College of Chemistry, Fuzhou University, Fuzhou 350002, China; qiangwan94@gmail.com
* Correspondence: zhoushulan2009@126.com (S.Z.); slin@fzu.edu.cn (S.L.)

Abstract: In this work, the H_2 dissociation and acetylene hydrogenation on Cu doped CeO_2(111) were studied using density functional theory calculations. The results indicated that Cu doping promotes the formation of oxygen vacancy (O_v) which creates Cu/O and Ce/O frustrated Lewis pairs (FLPs). With the help of Cu/O FLP, H_2 dissociation can firstly proceed via a heterolytic mechanism to produce Cu-H and O-H by overcoming a barrier of 0.40 eV. The H on Cu can facilely migrate to a nearby oxygen to form another O-H species with a barrier of 0.43 eV. The rate-determining barrier is lower than that for homolytic dissociation of H_2 which produces two O-H species. C_2H_2 hydrogenation can proceed with a rate-determining barrier of 1.00 eV at the presence of Cu-H and O-H species., While C_2H_2 can be catalyzed by two O-H groups with a rate-determining barrier of 1.06 eV, which is significantly lower than that (2.86 eV) of C_2H_2 hydrogenated by O-H groups on the bare CeO_2(111), showing the high activity of Cu doped CeO_2(111) for acetylene hydrogenation. In addition, the rate-determining barrier of C_2H_4 further hydrogenated by two O-H groups is 1.53 eV, much higher than its desorption energy (0.72 eV), suggesting the high selectivity of Cu doped CeO_2(111) for C_2H_2 partial hydrogenation. This provides new insights to develop effective hydrogenation catalysts based on metal oxide.

Keywords: acetylene hydrogenation; oxygen vacancy; Cu doped CeO_2(111); frustrated Lewis pairs; DFT

check for updates

Citation: Zhou, S.; Wan, Q.; Lin, S. Cu/O Frustrated Lewis Pairs on Cu Doped CeO_2(111) for Acetylene Hydrogenation: A First-Principles Study. *Catalysts* **2022**, *12*, 74. https://doi.org/10.3390/catal12010074

Academic Editors: C. Heath Turner, Tibor Szilvási, Wei An and Yaqiong Su

Received: 23 December 2021
Accepted: 8 January 2022
Published: 10 January 2022

1. Introduction

Partial hydrogenation of acetylene in excess of ethylene is a crucial industry process in the purifying of ethylene produced in steam cracker since polymerization catalysts can be poisoned by acetylene [1]. Pd based catalysts are commonly used in this reaction, which have been extensively studied over the past decades [2–4]. However, the lower selectivity caused by over-hydrogenation and oligomerization is a long-standing concern [1,4,5]. The high cost of Pd triggers intense interest in searching for low-cost catalysts with high performance.

Ceria (CeO_2) as the catalyst or catalyst support plays a vital role in the field of heterogeneous catalysis, such as CO oxidation [6–9], methane reforming [7], propane dehydrogenation [10], reduction of N_2 [11,12], and CO_2 conversion [13], have been extensively studied. Recently, CeO_2 has emerged as an efficient catalyst for hydrogenation reactions, attracting more and more attention from both experimental and theoretical investigations [14–25]. Due to its high selectivity for alkyne hydrogenation to target alkene, CeO_2 has potential to be the alternative of Pd based catalysts [20].

The surface oxygens were previously considered as the active sites for acetylene hydrogenation based on the density functional theory (DFT) study on CeO_2(111) [26]. It was suggested that acetylene be catalyzed by the homolytic products of H_2 dissociation (O-H groups) but with an extremely high barrier of 2.86 eV for the second hydrogenation step.

Subsequently, a concerted mechanism was reported by García-Melchor et al., suggesting that propyne is simultaneously hydrogenated by a surface O-H and a H atom in gas H_2 with a barrier of about 1.88 eV [27]. Recently, a new mechanism on CeO_2(110), CeO_2(100), and CeO_2(111) was proposed based on the presence of oxygen vacancies (O_vs) [19,28,29]. The Frustrated Lewis acid–base pairs (FLPs), namely, the combination of Lewis acid and Lewis base sterically encumbered, play a vital role in the hydrogenation process due to their high activity in activation of small molecules [30–37]. For example, on CeO_2(111), the acetylene is hydrogenated by the Ce-H and O-H groups generated by H_2 heterolytic dissociation with a barrier of 0.70 eV, significantly lower than the previous value (2.86 eV) [26]. The FLP formed by the Ce exposed by O_vs and the surface oxygen promotes the H_2 heterolytic dissociation with a much lower barrier (0.52 eV) than that (about 1 eV) [38,39] of homolytic dissociation. More importantly, the Ce sites can help stabilizing the Ce-H hydride and avoiding the strong adsorption of C_2H_3 intermediate, thus leading to a lower hydrogenation barrier. This mechanism concerning the involvement of Ce-H hydride in acetylene hydrogenation was partly confirmed by the experimental observations by different techniques such as neutron scattering spectroscopy [14,40].

Although CeO_2 shows high selectivity for alkyne hydrogenation, the reaction requires a high temperature >500 K [20]. Therefore, it is highly desirable to enhance the catalytic activity of CeO_2 for alkyne hydrogenation. Riley et al. reported that Ni can be used as a dopant to create O_vs and improve the activity of CeO_2 for acetylene hydrogenation [28]. They found that the reaction temperature on Ni doped CeO_2 is significantly lower than that on bare CeO_2, in which Ni did not take part in the reaction but acted as a promoter by leading to more active sites via increasing the O_vs. Moreover, the catalytic activity for alkyne hydrogenation can also be enhanced by introducing Ga into CeO_2 lattice [41]. The Ga/O FLP led by Ga doping plays a vital role in H_2 dissociation and reducing the rate-determining barrier of hydrogenation [42]. Cu based catalysts were found to show promising selectivity in hydrogenation reactions [43–46]. In addition, the previous studies indicated that Cu dopant [47,48] can enhance the formation of oxygen vacancies over CeO_2, which might be helpful to improve the catalytic activity of CeO_2 for hydrogenation. However, the catalytic role of Cu dopant in the hydrogenation on Cu doped CeO_2(111) (denoted as Cu-CeO_2(111)) is not clear.

In this work, since CeO_2(111) is the most stable facet, the mechanism of H_2 dissociation and C_2H_2 hydrogenation on Cu-CeO_2(111) was studied through DFT calculations. The results indicated that Cu doping leads to the formation of Cu/O FLP which promotes the dissociation of H_2 and C_2H_2 hydrogenation can be catalyzed by two surface O-H groups with the assistance of the Cu single atom on Cu-CeO_2(111). This is organized as follows: Section 2 gives the computational details. The results and discussion are shown in Section 3. The conclusions are presented in the final section.

2. Computational Details

All calculations were performed using spin-polarized DFT as implemented in Vienna ab initio simulation package (VASP) [49,50]. The gradient-corrected Perdew–Burke–Ernzerhof (PBE) approximation was used to treat the exchange–correlation potential [51]. The wave functions for the valence electrons were expanded in plane waves with a cutoff energy of 400 eV, while the core electrons were represented by projector augmented-wave (PAW) method [52]. DFT-D3 method of Grimme was employed to describe the van der Waals interaction [53]. The DFT + U method with an effective U = 4.5 eV was used to improve the description of Ce f states in ceria [54–56]. A periodic slab with a $p(3 \times 3)$ unit cell was selected to simulate the CeO_2(111) surface. The CeO_2(111) slab consists of nine atomic layers and a vacuum space of 14 Å. For all calculations, the atoms in top six layers were fully relaxed while those in the bottom three layers were fixed at their bulk positions. For Cu-CeO_2(111), a surface Ce was replaced by a Cu. A $1 \times 1 \times 1$ Monkhorst−Pack mesh k-point was adopted in Brillouin zone integration, which was tested to converge. Transition states of related elementary reaction steps were determined using the climbing

image nudged elastic band (CI-NEB) method [57]. The convergence criteria for forces on each iron and for energy is set to 0.05 eV/Å and 10^{-4} eV, respectively. The adsorption energy (E_{ads}) was computed using the equation of E_{ads} = E(adsorbate + surface) − E(free molecule) − E(free surface). The formation energy of an O_v was obtained by the following equation: E_f = E(slab-O_v) + 1/2E(O_2) − E(slab).

Derived from homogeneous catalysis, the combination of Lewis acids and bases hindered by steric hindrance can form FLPs [30,31] which are found to be very efficient in activating small molecules such as CO_2 and H_2 [32–37]. For CeO_2, a heterogeneous catalyst, the surface Ce and O atom can be considered as Lewis acid and base, respectively. In the presence of surface defects, some of the Lewis acid and base sites can be sterically separated, generating solid FLPs [19,28,29,32,42,58].

3. Results and Discussion

3.1. Geometry of Cu-CeO_2(111) without and with One O_v

The most stable geometry of Cu-CeO_2(111) are shown in Figure 1a. The Cu atom interacts with one surface oxygen (O1) and three subsurface oxygens (O2, O3, and O4), forming a square planar with the Cu-O1, Cu-O2, Cu-O3, and Cu-O4 distances of 1.97, 1.92, 1.93, and 1.98 Å, respectively. This is consistent with the result calculated by Guo et al. [59]. The lattice distortion leads to two 2-fold Os, which are easy to form O_vs. The calculated formation energy of an O_v by a 2-fold O is −0.15 eV, indicating this process is thermally favorable. This is similar to the situation in Ni doped CeO_2(111) [28].

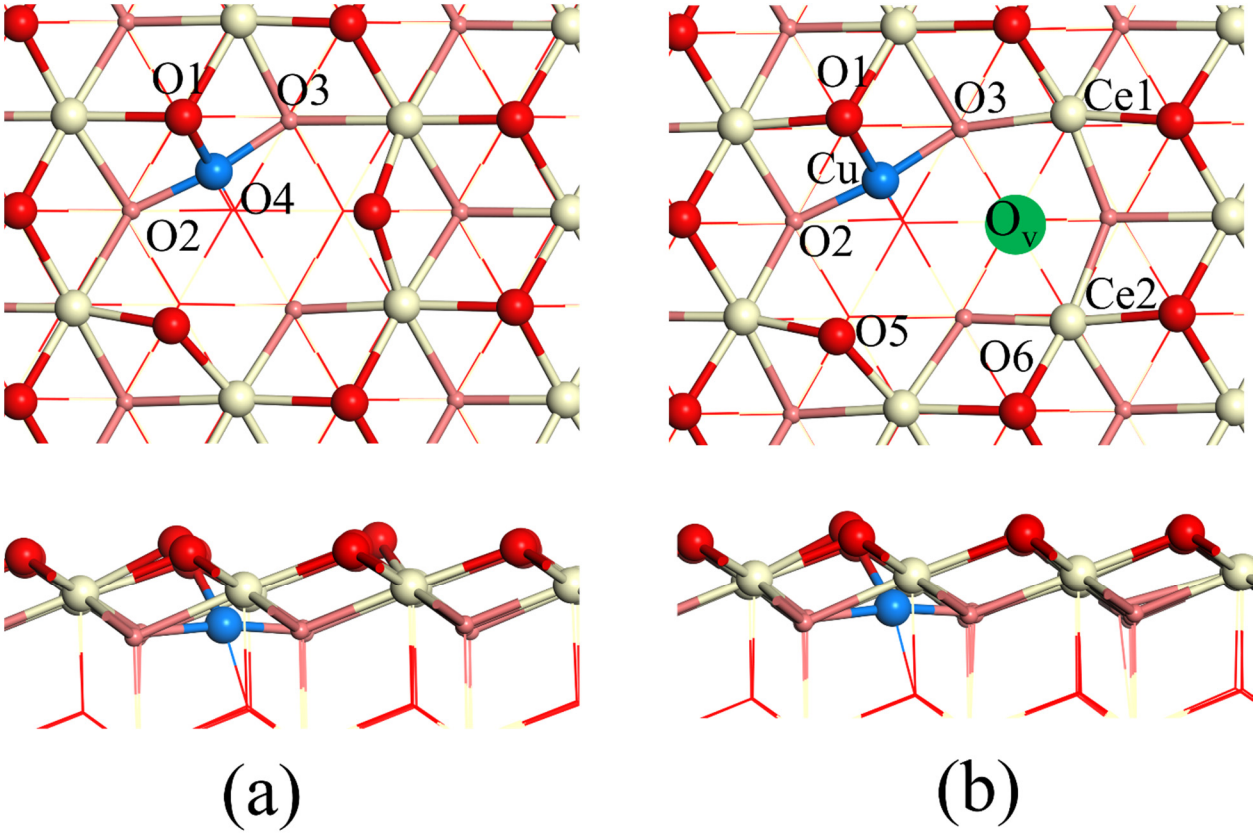

Figure 1. Top and side views of Cu-CeO_2(111) without and with an oxygen vacancy. (**a**) Cu-CeO_2(111); (**b**) Cu-CeO_2(111)-O_v. The position of O_v is indicated by the green ball. Cu/O5, Cu/O6 and Ce1/O6 form potential FLPs. Color scheme: Cu, blue; Ce, yellow; oxygen, red; subsurface oxygen, light red.

The optimized geometry of Cu-CeO_2(111) with one O_v (denoted as Cu-CeO_2(111)-O_v) is shown in Figure 1b. For Cu-CeO_2(111)-O_v, it was found that Cu and O5 are sterically separated by 3.64 Å, forming a standard FLP. The Cu and nonadjacent O6 with a distance

of 3.24 Å also fall in the domain of FLP (denoted as Cu/O6 FLP). In addition, the distance of the nonadjacent Ce1 and O6 is 4.66 Å, forming another FLP candidate (denoted as Ce/O6 FLP).

3.2. H_2 Dissociation on Cu-CeO_2(111)-O_v

As aforementioned, on Cu-CeO_2(111)-O_v, there are three possible FLPs (Cu/O5, Cu/O6, and Ce/O6 FLPs) which might catalyze the heterolytic dissociation of H_2. In order to understand the activity of these FLPs, H_2 dissociation on Cu/O5 FLP (Path I), Ce/O6 FLP (Path II), and Cu/O6 FLP (Path III) were considered. The reaction and activation energies are listed in Table 1 and the corresponding geometries of initial state (IS), transition state (TS), and final state (FS) are presented in Figure 2a–i.

Table 1. Reaction energies (ΔE) and activation energies (E_a) for the elementary steps involved in the H_2 dissociation, C_2H_2 and C_2H_4 hydrogenation on Cu-CeO_2(111)-O_v. The unit of energies is in eV. Here * denotes the slab.

Reactions	C_2H_2		C_2H_4	
	ΔE	E_a	ΔE	E_a
H_2+* → H_2* (I)	−0.19	-	−0.19	-
H_2*→H*(O) + H*(Ce) (III)	−0.66	0.40	−0.66	0.40
H*(O) + H*(Ce) → 2H* (O) (V)	−1.15	0.43	−1.15	0.43
C_2H_2(g) + 2H*(O)+* → C_2H_2* + 2H* (VI)	−0.22	-	-	-
C_2H_4(g) + 2H*(O)+* → C_2H_4* + 2H*	-	-	−0.65	-
C_2H_2* + 2H*(O) → C_2H_3* + H*(O) (VIII)	−0.44	0.69	-	-
C_2H_4(g) + 2H*(O) → C_2H_5* + H*(O) (g2)	-	-	0.64	1.53
C_2H_3* + H*(O) → C_2H_4* (X)	0.73	1.06	-	-
C_2H_5* + H*(O) → C_2H_6* (g4)	-	-	0.46	1.33

For Path I, the corresponding geometries are shown in Figure 2a–c. H_2 weakly adsorbs on the surface with the adsorption energy of −0.19 eV with the H-H distance of 0.76 Å. In TS (Figure 2b), the bond distance of H1-O and Cu-H2 decreased to 1.29 and 1.77 Å, respectively, while the bond length of H1-H2 increased to 0.98 Å. Finally, it dissociates into H-O and Cu-H groups (Figure 2c) via a heterolytic path on Cu/O5 FLP by overcoming a barrier of 0.40 eV, which is about 0.6 eV lower than that of homolytic dissociation on CeO_2(111) [38,39] and is also about 0.1 eV lower than that of heterolytic dissociation on Ni doped CeO_2(111) with an O_v [28]. This suggests that Cu/O5 FLP plays an important role in the stabilization of TS. Interestingly, the interaction of H_2 with Cu leads to the structural transformation from CuO_4 to CuO_3, which facilitates the formation of Cu-H and O-H groups. The H_2 dissociation via Path I releases an energy of 0.66 eV, showing that it is a thermally favorable process.

For Path II, the geometries of IS, TS and FS are shown in Figure 2d–f. H_2 dissociation proceeds on Ce/O6 sites through a heterolytic path. Before dissociation, H_2 weakly adsorbs on the O_v with the adsorption energy of −0.24 eV. In TS (Figure 2e), the distance between H1 and H2 is elongated to 1.02 Å from 0.74 Å in its initial state, while the distances of H1-O2, H1-Ce1, and H2-Ce1 reduced to 1.27, 2.33, and 2.47 Å, respectively. The calculated barrier of H_2 dissociation on Ce/O sites is 0.51 eV, which is very close to those on bare CeO_2(111)-O_v (0.52 eV) and on Ni-CeO_2(111)-O_v (0.50 eV) [28]. However, the barrier is about 0.16 eV higher than that (0.40 eV) on Cu/O5 FLP, indicating that Cu/O5 FLP is more active than Ce/O6 FLP for H_2 dissociation. In FS (Figure 2f), H_2 breaks into O-H and Ce-H hydride. This process is slightly endothermic (0.08 eV).

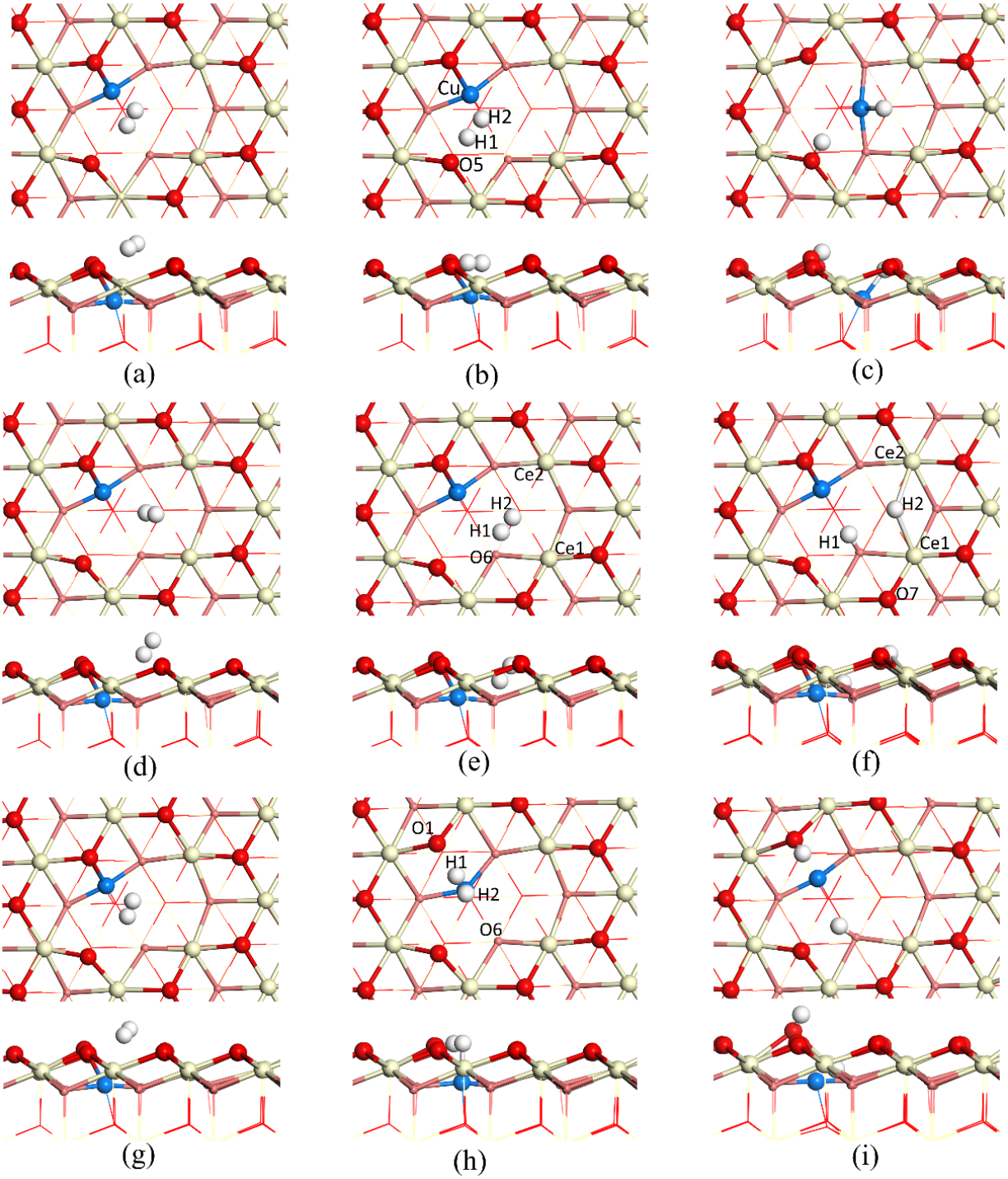

Figure 2. Top and side views for H_2 dissociation on Cu-CeO_2(111)-O_v. (**a**) H_2* (I), (**b**) TS (II) and (**c**) heterolytic products (H*-O* + H*-Cu) (III) for Path I via Cu/O5 FLP; (**d**) H_2*, (**e**) TS and (**f**) heterolytic products (H*-O* + H*-Ce) for Path II via Ce/O6 FLP and (**g**) H_2*, (**h**) TS and (**i**) homolytic products (H*-O* + H*-O) for Path III via Cu/O6. Color scheme: Cu, blue; Ce, yellow; oxygen, red; subsurface oxygen, light red; H, white.

Besides the above paths, there is another reaction pathway (Path III) in which H_2 was expected to dissociate on Cu/O6 FLP following the heterolytic mechanism. The corresponding geometries are displayed in Figure 2g–i. In this case, H_2 is physically adsorbed on the surface with the adsorption energy of −0.19 eV. Observing the geometry of TS (Figure 2h), it is found that the distance of H1-H2 has increased to 0.86 Å and the

distances of O1-H1, Cu-H1, and Cu-H2 decreased to 1.59, 1.83, and 1.71 Å, respectively, while the distance of O6-H2 is more than 3 Å. This suggests that the Cu/O6 is not an effective FLP for catalyzing H_2 dissociation. Finally, we can see H_2 dissociates into two O-H groups (Figure 2i), implying a homolytic mechanism. The calculated barrier is 0.54 eV.

Comparing the barriers of H_2 dissociation via the above three discussed reaction paths, it is found that the barrier (0.40 eV) of Path I on Cu/O5 FLP is not only lower than that (0.51 eV) on Ce/O6 FLP in Path II and also lower than that (0.54 eV) in Path III, showing that H_2 prefers to dissociate through Path I on Cu/O5 FLP to form Cu-H hydride and O-H groups.

To understand the stability of the Cu-H hydride, the migration of hydride H to a neighbor O is calculated. The geometries of IS, TS and FS are given in Figure 3. The calculated barrier is 0.43 eV, implying that the migration of hydride H is not difficult. This barrier is also lower than those for Path II (0.52 eV) and Path III (0.54 eV), indicating H_2 can firstly dissociate via a heterolytic mechanism (Path I) and then the heterolytic products transform to homolytic ones with a barrier of 0.43 eV. This is different from the case of Ni doped CeO_2(111) with one O_v, on which the hydride is very stable since the migration of hydride H needs to overcome a relatively large barrier of 0.87 eV [28]. Therefore, for Cu-CeO_2(111)-O_v, the homolytic products (O-H groups) from H_2 dissociation might be the active species for the subsequent C_2H_2 hydrogenation.

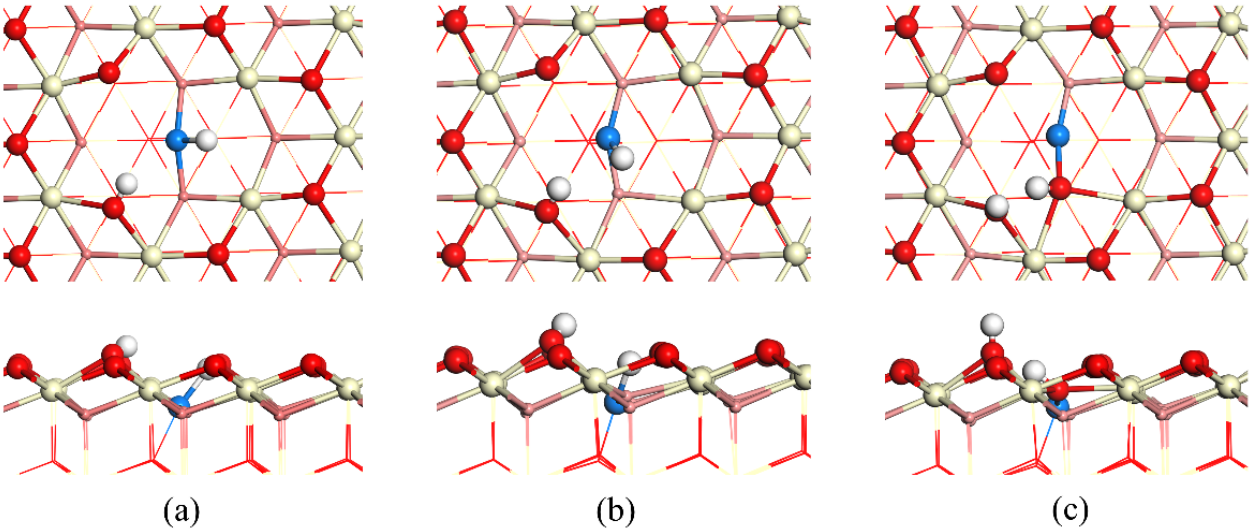

Figure 3. Top and side views of the geometries for the migration of H adsorbed on Cu to a nearby surface oxygen. (**a**) IS (III), (**b**) TS (IV), and (**c**) FS (V). Color scheme: Cu, blue; Ce, yellow; oxygen, red; subsurface oxygen, light red; H, white.

3.3. Acetylene Hydrogenation on Cu-CeO_2(111)-O_v

The reaction process of acetylene catalyzed by the Cu-H and O-H groups was firstly studied (denoted as Path I). The corresponding geometries are shown in Figure 4a–e. C_2H_2 adsorbs on the surface with an adsorption energy of −0.56 eV. The C_2H_2 can capture the hydride H to form C_2H_3 with a barrier of 0.40 eV, releasing an energy of −1.46 eV. The produced C_2H_3 intermediate bonds to the Cu site with an adsorption energy of −2.01 eV and then reacts with the hydroxyl H to form C_2H_4 with a rate-determining barrier of 1.00 eV. This process is endothermic (0.67 eV).

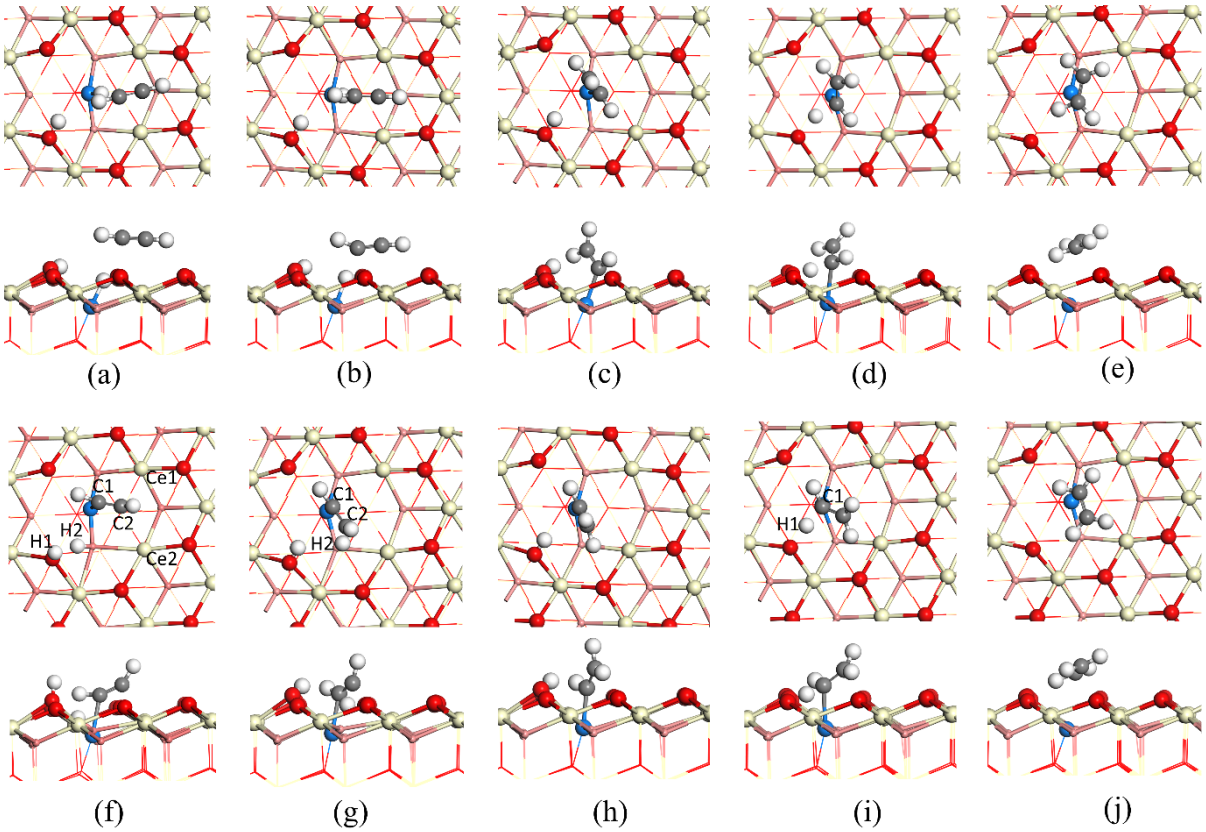

Figure 4. Top and side views of acetylene hydrogenation on Cu-CeO_2(111)-O_v. (**a**–**e**) C_2H_2 catalyzed by heterolytic products (Path I). (**f**–**j**) C_2H_2 catalyzed by homolytic products (Path II). (**a**) C_2H_2* + 2H (H*-Cu + H*-O) (VI); (**b**) TS (VII), (**c**) C_2H_3* + H*-O (VIII); (**d**) TS (IX) and (**e**) C_2H_4* (X) for Path I. (**f**) C_2H_2* + 2H (H*-O + H*-O) (VI); (**g**) TS (VII); (**h**) C_2H_3* + H*-O (VIII); (**i**) TS (IX); (**j**) C_2H_4* (X). Color scheme: Cu, blue; Ce, yellow; oxygen, red; subsurface oxygen, light red; C, grey; H, white.

Based on the above results, it is possible that the migration of hydride H can take place before C_2H_2 hydrogenation because its barrier (0.43 eV) is very close to that (0.40 eV) of the first hydrogenation step and much lower than that (1.00 eV) of the second hydrogenation step. This is different with the case of Ni doped CeO_2(111)-O_v, in which, the hydride is very stable due to the migration barrier of 0.87 eV is much higher than the first and second hydrogenation barriers (0.13 and 0.62 eV) [28].

To further investigate the possibility of acetylene hydrogenation catalyzed by the O-H groups and explore the role Cu dopant in the catalysis, the hydrogenation process was calculated (denoted as Path II). The corresponding geometries are depicted in Figure 4f–j and the reaction and activation energies are shown in Table 1.

As indicated in Figure 4f, at first, C_2H_2 adsorbs on the Cu atom with an adsorption energy of −0.22 eV. The distance of C1-Cu, C1-C2, C2-Ce1, and C2-Ce2 is 2.10, 1.26, 2.96, and 3.08 Å, respectively. Then C_2H_2* (Figure 4f) reacted with the H2 adsorbed on the neighbor O to form C_2H_3 species by overcoming a barrier of 0.69 eV. In the TS (Figure 4g), the distance of C2-H2 and C1-Cu decreased to 1.37 and 1.98 Å, respectively, while the distance of H2-O increased to 1.26 Å. This implies that Cu can help to stabilize the TS. The C_2H_3 intermediate is binding to the Cu site with an adsorption energy of −2.19 eV and with a C-Cu distance of 1.91 Å. Subsequently, C_2H_3 can trap the H (H1) on another O-H group to generate the C_2H_4 product by surpassing a barrier of 1.06 eV. In the TS (Figure 4i), the distance of C1-Cu and H1-O enlarged to 1.38 and 2.08 Å, respectively, and the distance of C1-H2 decreased to 1.30 Å. The second hydrogenation step is endothermic (0.73 eV). In the FS, C_2H_4 (Figure 4j) adsorbs on the surface with the C1-Cu and C2-Cu distance of 2.90 and 3.36 Å, respectively. In this configuration, the Cu connects with three subsurface Os,

forming a CuO_3 configuration. From Figure 5, one can see that CuO_3 can facilely transform to a square planar CuO_4 configuration via the migration of Cu with a minor barrier of 0.13 eV. In the other words, the Cu-CeO_2(111)-O_v catalyst can recover itself, revealing the importance of structural dynamics during the catalysis.

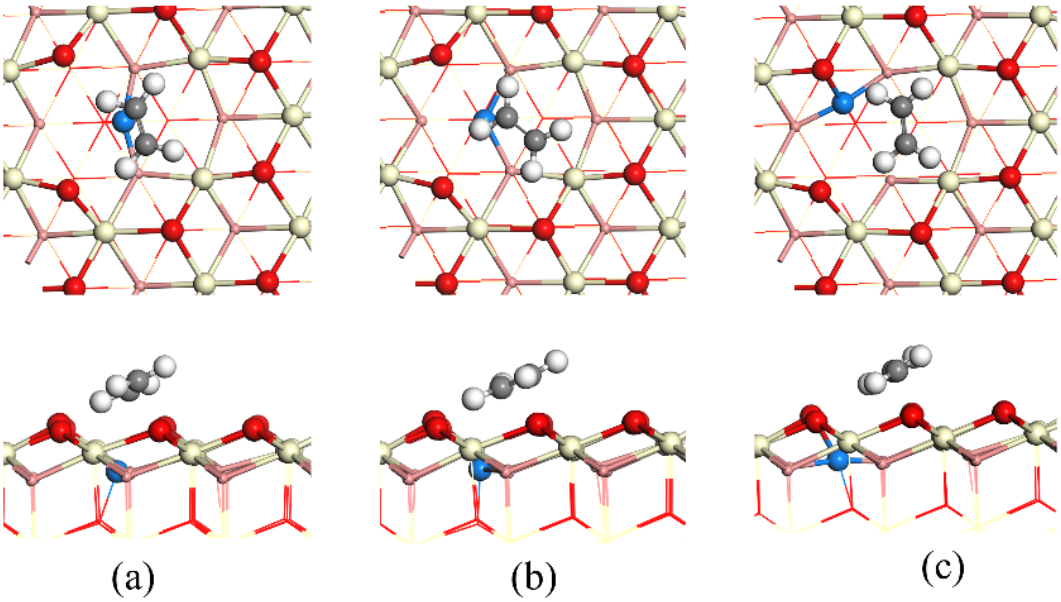

Figure 5. Top and side views of IS (**a**), TS (**b**) and FS (**c**) for the migration of Cu. Color scheme: Cu, blue; Ce, yellow; oxygen, red; subsurface oxygen, light red; C, grey; H, white.

In order to investigate the possibility of C_2H_4 hydrogenated by the O-H groups, the hydrogenation process of C_2H_4 was also studied. The reaction and activation energies are also shown in Table 1 and the corresponding geometries are given in Figure 6a–e. The C_2H_4 adsorbs over the surface with an adsorption energy of −0.65 eV. It can react with the H on the O to form C_2H_5 by surpassing a barrier of 1.53 eV, which is much higher than that the desorption energy of C_2H_4 (0.72 eV). C_2H_5 adsorbs on the Cu site with an adsorption energy of −1.27 eV and with the C-Cu distance of 2.00 Å. Then C_2H_5 can be further hydrogenated to C_2H_6 by another surface H adsorbed on O with a barrier of 1.33 eV. The results indicate that the barriers for both the first and second steps of C_2H_4 hydrogenation are much higher than the desorption energy (0.72 eV) of C_2H_4 implying a good selectivity of Cu-CeO_2(111)-O_v for C_2H_2 partial hydrogenation.

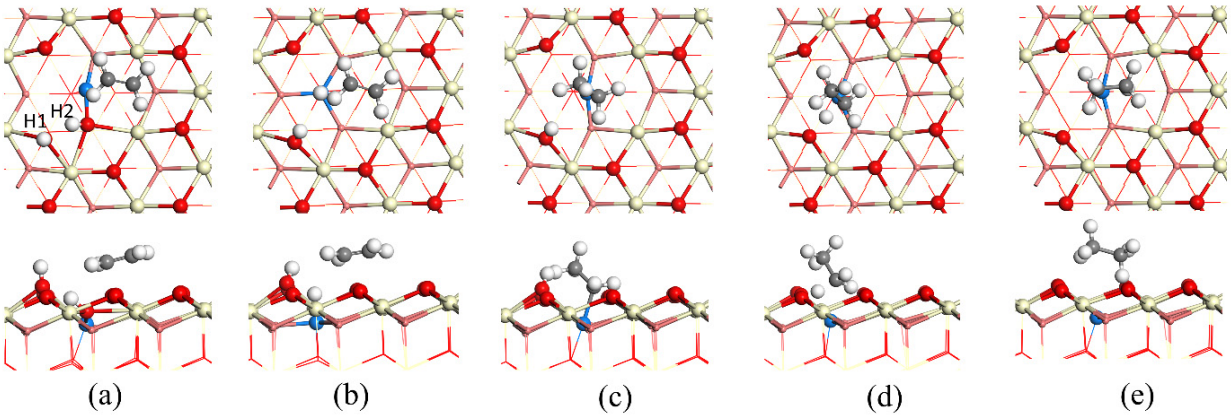

Figure 6. Top and side views of C_2H_4 hydrogenation on Cu-CeO_2(111)-O_v. (**a**) C_2H_4* + 2H*-O; (**b**) TS (g1); (**c**) C_2H_5* + H*-O (g2); (**d**) TS (g3); and (**e**) C_2H_6* (g4). Color scheme: Cu, blue; Ce, yellow; oxygen, red; subsurface oxygen, light red; C, grey; H, white.

Finally, the whole energy pathway is summarized with the energy profiles of C_2H_2 and C_2H_4 hydrogenation shown in Figure 7. The results of C_2H_2 hydrogenation on $CeO_2(111)$-O_v calculated by some of our current authors [28] and on $CeO_2(111)$ calculated by Carrasco et al. [26]. are also shown in Figure 7. For C_2H_2 catalyzed by the heterolytic products (Path I), the barrier of the second hydrogenation step is 1.00 eV, which is not only higher than the barrier (0.40 eV) of H_2 heterolytic dissociation but also higher than that (0.40 eV) of the first hydrogenation step. Hence, the rate-determining barrier is 1.00 eV, which is much higher than the migration barrier (0.43 eV) of hydride H, suggesting the formation of homolytic products is very possible during the hydrogenation process. For C_2H_2 catalyzed by the homolytic products (Path II), the barrier of the second hydrogenation step is 1.06 eV. It is higher than that (0.69 eV) of the first hydrogenation step and that (0.43 eV) of H_2 homolytic dissociation, showing the second hydrogenation step controls the whole reaction rate of C_2H_2 partial hydrogenation on Cu-$CeO_2(111)$-O_v. Comparing the results with those on $CeO_2(111)$-O_v and $CeO_2(111)$, it is found that the barrier of 1.06 eV is higher than that (0.70 eV) [28] on $CeO_2(111)$-O_v, however, it is 1.80 eV lower than that (2.86 eV) [26] catalyzed by homolytic products on bare $CeO_2(111)$, suggesting the activity of CeO_2 is effectively enhanced by the Cu dopant. Cu plays a vital role in reducing the barrier of second hydrogenation step, which avoids the strong adsorption of C_2H_3 intermediate. For C_2H_4, the barrier of the first hydrogenation step is 1.53 eV, higher than that (0.43 eV) of H_2 dissociation and that (1.33 eV) of the second hydrogenation step, suggesting the addition of the first hydrogen is the rate-determining step. This barrier is 0.81 eV higher than the desorption energy (0.72 eV) of C_2H_4, implying a high selectivity of Cu-$CeO_2(111)$-O_v for C_2H_2 partial hydrogenation.

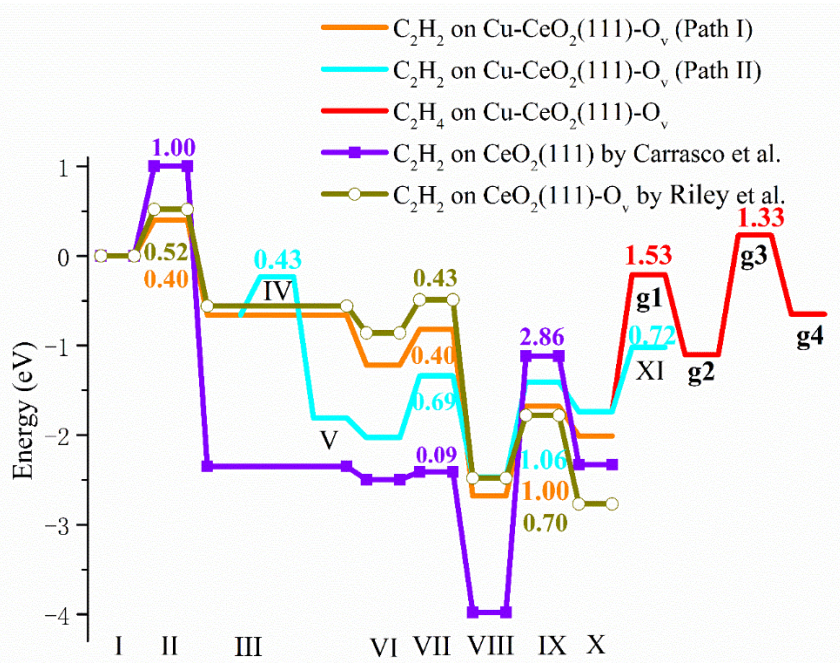

Figure 7. Calculated energy profiles of C_2H_2 and C_2H_4 hydrogenation on Cu-$CeO_2(111)$-O_v. The results of C_2H_2 hydrogenation on $CeO_2(111)$-O_v by Riley et al. and on $CeO_2(111)$ by Carrasco et al. are also given. The data given in the Figure indicate the activation energies (eV) of TSs. I: H_2*, II: TS for H_2 dissociation, III: (H*-O + H*-Cu) for Cu-$CeO_2(111)$-O_v, (H*-O + H*-Ce) for $CeO_2(111)$-O_v and (H*-O + H*-O) for $CeO_2(111)$ IV: TS for H migration on Cu-$CeO_2(111)$-O_v, V: homolytic products of 2H* (H*-O + H*-O) for Cu-$CeO_2(111)$-O_v; VI: C_2H_2* + 2H (H*-Cu/Ce + H*-O) for Path I and $CeO_2(111)$-O_v, C_2H_2* + 2H (H*-O + H*-O) for Path II and $CeO_2(111)$, VII: TS for first hydrogenation step of C_2H_2, VIII: H* + C_2H_3*, IX: TS for second hydrogenation step of C_2H_2, X: C_2H_4*, XI: C_2H_4, g1: TS for the first hydrogenation step of C_2H_4, g2: H* + C_2H_5*, g3: TS for the second hydrogenation step of C_2H_4, g4: C_2H_6*. Here * denotes the adsorption state. The notes (I, II, etc.) of states are consistent with those in Figures 1–6 and Table 1.

4. Conclusions

In this work, the H_2 dissociation and C_2H_2 hydrogenation on Cu-CeO_2(111)-O_v were studied by density functional theory calculations. It is found that Cu doping leads to the spontaneous formation of O_v, generating Cu/O FLP which promotes the H_2 dissociation and acetylene hydrogenation. On Cu-CeO_2(111)-O_v, H_2 can firstly dissociate to Cu-H and O-H groups via a heterolytic mechanism by surpassing a barrier of 0.40 eV. The migration of hydride H on Cu leads to the homolytic product of two O-H groups by overcoming a barrier of 0.43 eV, which is much lower than that (about 1 eV) of homolytic dissociation of H_2 on bare CeO_2(111). In addition, the results indicate that C_2H_2 can be catalyzed either by the heterolytic products (Cu-H and O-H) or homolytic products (O-Hs). For C_2H_2 hydrogenated by the heterolytic products, the addition of the second hydrogen controls the whole reaction rate. The rate-determining barrier is 1.00 eV, leading to a higher possibility of hydride H migration to form homolytic products. For C_2H_2 hydrogenated by the homolytic products, the reaction rate is determined by the second hydrogenation step with a barrier of 1.06 eV, which is about 1.80 eV lower than that (2.86 eV) of C_2H_2 hydrogenated by O-H groups on CeO_2(111), showing the efficiency of Cu-CeO_2(111)-O_v for C_2H_2 hydrogenation. Moreover, the desorption energy (0.72 eV) of C_2H_4 is significantly lower than the rate-determining barrier (1.53 eV) for C_2H_4 hydrogenation, suggesting a high selectivity of Cu-CeO_2(111)-O_v for acetylene partial hydrogenation. Cu dopant plays a vital role in promoting the activity of CeO_2 for acetylene hydrogenation. Firstly, it creates the Cu/O FLP, the active site for H_2 dissociation and C_2H_2 hydrogenation. Secondly, it provides the adsorption site for C_2H_3 intermediate, avoiding the strong adsorption on the surface O, thus reducing the energy barrier for the second step of C_2H_2 hydrogenation. This work provides valuable insights to design effective catalysts based on metal oxide.

Author Contributions: Conceptualization, S.Z. and S.L.; methodology, S.Z. and Q.W.; software, S.Z.; formal analysis, S.Z., Q.W. and S.L.; investigation, S.Z.; data curation, S.Z.; writing—original draft preparation, S.Z.; writing—review and editing, S.Z., Q.W. and S.L. All authors have read and agreed to the published version of the manuscript.

Funding: This research was funded by the National Natural Science Foundation of China (Grant no. 21962007 to S.Z., and 21973013 to S.L.), Natural Science Foundation of Jiangxi Province (Grant no. 2020BABL203009 to S.Z.), Foundation of Jiangxi Educational Committee (Grant no. GJJ190697 to S.Z.), and Qishan Scholarship Program of Fuzhou University (Grant no. XRC-17055 to S.L.), the National Natural Science Foundation of Fujian Province, China (Grant no. 2020J02025 to S.L.), and the "Chuying Program" for the Top Young Talents of Fujian Province.

Data Availability Statement: Not available.

Conflicts of Interest: The authors declare no conflict of interest.

References

1. Bond, G.C. *Metal-Catalysed Reactions of Hydrocarbons*; Fundamental and Applied Catalysis Series; Springer: New York, NY, USA, 2005; pp. 395–435.
2. Bridier, B.; López, N.; Pérez-Ramírez, J. Molecular understanding of alkyne hydrogenation for the design of selective catalysts. *Dalton Trans.* **2010**, *39*, 8412–8419. [CrossRef]
3. Teschner, D.; Borsodi, J.; Wootsch, A.; Révay, Z.; Hävecker, M.; Knop-Gericke, A.; Jackson, S.D.; Schlögl, R. The Roles of Subsurface Carbon and Hydrogen in Palladium-Catalyzed Alkyne Hydrogenation. *Science* **2008**, *320*, 86–89. [CrossRef]
4. Crespo-Quesada, M.; Cárdenas-Lizana, F.; Dessimoz, A.-L.; Kiwi-Minsker, L. Modern Trends in Catalyst and Process Design for Alkyne Hydrogenations. *ACS Catal.* **2012**, *2*, 1773–1786. [CrossRef]
5. Mitsudome, T.; Kaneda, K. Gold nanoparticle catalysts for selective hydrogenations. *Green Chem.* **2013**, *15*, 2636–2654. [CrossRef]
6. Feng, Y.; Wan, Q.; Xiong, H.; Zhou, S.; Chen, X.; Hernandez, X.I.P.; Wang, Y.; Lin, S.; Datye, A.K.; Guo, H. Correlating DFT Calculations with CO Oxidation Reactivity on Ga-Doped Pt/CeO_2 Single-Atom Catalysts. *J. Phys. Chem. C* **2018**, *122*, 22460–22468. [CrossRef]
7. Rodriguez, J.A.; Grinter, D.C.; Liu, Z.; Palomino, R.M.; Senanayake, S.D. Ceria-based model catalysts: Fundamental studies on the importance of the metal–ceria interface in CO oxidation, the water–gas shift, CO_2 hydrogenation, and methane and alcohol reforming. *Chem. Soc. Rev.* **2017**, *46*, 1824–1841. [CrossRef] [PubMed]

8. Kim, H.J.; Jang, M.G.; Shin, D.; Han, J.W. Design of Ceria Catalysts for Low-Temperature CO Oxidation. *ChemCatChem* **2020**, *12*, 11–26. [CrossRef]
9. Wan, Q.; Wei, F.; Wang, Y.; Wang, F.; Zhou, L.; Lin, S.; Xie, D.; Guo, H. Single atom detachment from Cu clusters, and diffusion and trapping on CeO_2(111): Implications in Ostwald ripening and atomic redispersion. *Nanoscale* **2018**, *10*, 17893–17901. [CrossRef]
10. Xiong, H.; Lin, S.; Goetze, J.; Pletcher, P.; Guo, H.; Kovarik, L.; Artyushkova, K.; Weckhuysen, B.M.; Datye, A.K. Thermally Stable and Regenerable Platinum–Tin Clusters for Propane Dehydrogenation Prepared by Atom Trapping on Ceria. *Angew. Chem. Int. Ed.* **2017**, *56*, 8986–8991. [CrossRef]
11. Qi, J.; Gao, L.; Wei, F.; Wan, Q.; Lin, S. Design of a High-Performance Electrocatalyst for N_2 Conversion to NH_3 by Trapping Single Metal Atoms on Stepped CeO_2. *ACS Appl. Mater. Interfaces* **2019**, *11*, 47525–47534. [CrossRef]
12. Qi, J.; Zhou, S.; Xie, K.; Lin, S. Catalytic role of assembled Ce Lewis acid sites over ceria for electrocatalytic conversion of dinitrogen to ammonia. *J. Energy Chem.* **2021**, *60*, 249–258. [CrossRef]
13. Chang, K.; Zhang, H.; Cheng, M.-J.; Lu, Q. Application of Ceria in CO_2 Conversion Catalysis. *ACS Catal.* **2020**, *10*, 613–631. [CrossRef]
14. Moon, J.; Cheng, Y.; Daemen, L.L.; Li, M.; Polo-Garzon, F.; Ramirez-Cuesta, A.J.; Wu, Z. Discriminating the Role of Surface Hydride and Hydroxyl for Acetylene Semihydrogenation over Ceria through In Situ Neutron and Infrared Spectroscopy. *ACS Catal.* **2020**, *10*, 5278–5287. [CrossRef]
15. Kammert, J.; Moon, J.; Wu, Z. A review of the interactions between ceria and H_2 and the applications to selective hydrogenation of alkynes. *Chin. J. Catal.* **2020**, *41*, 901–914. [CrossRef]
16. Huang, X.; Zhang, K.; Peng, B.; Wang, G.; Muhler, M.; Wang, F. Ceria-Based Materials for Thermocatalytic and Photocatalytic Organic Synthesis. *ACS Catal.* **2021**, *11*, 9618–9678. [CrossRef]
17. Montini, T.; Melchionna, M.; Monai, M.; Fornasiero, P. Fundamentals and Catalytic Applications of CeO_2-Based Materials. *Chem. Rev.* **2016**, *116*, 5987–6041. [CrossRef]
18. Zhang, Z.; Wang, Z.-Q.; Li, Z.; Zheng, W.-B.; Fan, L.; Zhang, J.; Hu, Y.-M.; Luo, M.-F.; Wu, X.-P.; Gong, X.-Q.; et al. Metal-Free Ceria Catalysis for Selective Hydrogenation of Crotonaldehyde. *ACS Catal.* **2020**, *10*, 14560–14566. [CrossRef]
19. Zhang, S.; Huang, Z.-Q.; Ma, Y.; Gao, W.; Li, J.; Cao, F.; Li, L.; Chang, C.-R.; Qu, Y. Solid frustrated-Lewis-pair catalysts constructed by regulations on surface defects of porous nanorods of CeO_2. *Nat. Commun.* **2017**, *8*, 15266. [CrossRef]
20. Vilé, G.; Bridier, B.; Wichert, J.; Pérez-Ramírez, J. Ceria in Hydrogenation Catalysis: High Selectivity in the Conversion of Alkynes to Olefins. *Angew. Chem. Int. Ed.* **2012**, *51*, 8620–8623. [CrossRef]
21. Vilé, G.; Colussi, S.; Krumeich, F.; Trovarelli, A.; Pérez-Ramírez, J. Opposite Face Sensitivity of CeO_2 in Hydrogenation and Oxidation Catalysis. *Angew. Chem. Int. Ed.* **2014**, *53*, 12069–12072. [CrossRef]
22. Cao, T.; You, R.; Li, Z.; Zhang, X.; Li, D.; Chen, S.; Zhang, Z.; Huang, W. Morphology-dependent CeO_2 catalysis in acetylene semihydrogenation reaction. *Appl. Surf. Sci.* **2020**, *501*, 144120. [CrossRef]
23. Cao, T.; You, R.; Zhang, X.; Chen, S.; Li, D.; Zhang, Z.; Huang, W. An in situ DRIFTS mechanistic study of CeO_2-catalyzed acetylene semihydrogenation reaction. *Phys. Chem. Chem. Phys.* **2018**, *20*, 9659–9670. [CrossRef]
24. Werner, K.; Weng, X.; Calaza, F.; Sterrer, M.; Kropp, T.; Paier, J.; Sauer, J.; Wilde, M.; Fukutani, K.; Shaikhutdinov, S.; et al. Toward an Understanding of Selective Alkyne Hydrogenation on Ceria: On the Impact of O Vacancies on H_2 Interaction with CeO_2(111). *J. Am. Chem. Soc.* **2017**, *139*, 17608–17616. [CrossRef] [PubMed]
25. Riley, C.; De La Riva, A.; Zhou, S.; Wan, Q.; Peterson, E.; Artyushkova, K.; Farahani, M.D.; Friedrich, H.; Burkemper, L.; Atudorei, N.; et al. Synthesis of Nickel-Doped Ceria Catalysts for Selective Acetylene Hydrogenation. *ChemCatChem* **2019**, *11*, 1526–1533. [CrossRef]
26. Carrasco, J.; Vilé, G.; Fernández-Torre, D.; Perez, R.; Pérez-Ramírez, J.; Ganduglia-Pirovano, M.V. Molecular-Level Understanding of CeO_2 as a Catalyst for Partial Alkyne Hydrogenation. *J. Phys. Chem. C* **2014**, *118*, 5352–5360. [CrossRef]
27. García-Melchor, M.; Bellarosa, L.; López, N. Unique Reaction Path in Heterogeneous Catalysis: The Concerted Semi-Hydrogenation of Propyne to Propene on CeO_2. *ACS Catal.* **2014**, *4*, 4015–4020. [CrossRef]
28. Riley, C.; Zhou, S.; Kunwar, D.; De La Riva, A.; Peterson, E.; Payne, R.; Gao, L.; Lin, S.; Guo, H.; Datye, A. Design of Effective Catalysts for Selective Alkyne Hydrogenation by Doping of Ceria with a Single-Atom Promotor. *J. Am. Chem. Soc.* **2018**, *140*, 12964–12973. [CrossRef]
29. Huang, Z.-Q.; Liu, L.-P.; Qi, S.; Zhang, S.; Qu, Y.; Chang, C.-R. Understanding All-Solid Frustrated-Lewis-Pair Sites on CeO_2 from Theoretical Perspectives. *ACS Catal.* **2018**, *8*, 546–554. [CrossRef]
30. Stephan, D.W. Frustrated Lewis Pairs. *J. Am. Chem. Soc.* **2015**, *137*, 10018–10032. [CrossRef] [PubMed]
31. Stephan, D.W. Frustrated Lewis Pairs: From Concept to Catalysis. *Acc. Chem. Res.* **2015**, *48*, 306–316. [CrossRef]
32. Wan, Q.; Li, J.; Jiang, R.; Lin, S. Construction of frustrated Lewis pairs on carbon nitride nanosheets for catalytic hydrogenation of acetylene. *Phys. Chem. Chem. Phys.* **2021**, *23*, 24349–24356. [CrossRef] [PubMed]
33. Chen, Z.; Zhao, J.; Zhao, J.; Chen, Z.; Yin, L. Frustrated Lewis pairs photocatalyst for visible light-driven reduction of CO to multi-carbon chemicals. *Nanoscale* **2019**, *11*, 20777–20784. [CrossRef]
34. Zhao, J.; Liu, X.; Chen, Z. Frustrated Lewis Pair Catalysts in Two Dimensions: B/Al-Doped Phosphorenes as Promising Catalysts for Hydrogenation of Small Unsaturated Molecules. *ACS Catal.* **2017**, *7*, 766–771. [CrossRef]
35. Sun, X.; Li, B.; Liu, T.; Song, J.; Su, D.S. Designing graphene as a new frustrated Lewis pair catalyst for hydrogen activation by co-doping. *Phys. Chem. Chem. Phys.* **2016**, *18*, 11120–11124. [CrossRef] [PubMed]

36. Lee, H.; Choi, Y.N.; Lim, D.; Rahman, M.; Kim, Y.; Cho, I.H.; Kang, H.W.; Seo, J.; Jeon, C.; Yoon, K.B. Formation of Frustrated Lewis Pairs in Pt_x-Loaded Zeolite NaY. *Angew. Chem. Int. Ed.* **2015**, *54*, 13080–13084. [CrossRef] [PubMed]
37. Ghuman, K.; Hoch, L.B.; Wood, T.E.; Mims, C.A.; Singh, C.V.; Ozin, G.A. Surface Analogues of Molecular Frustrated Lewis Pairs in Heterogeneous CO_2 Hydrogenation Catalysis. *ACS Catal.* **2016**, *6*, 5764–5770. [CrossRef]
38. García-Melchor, M.; López, N. Homolytic Products from Heterolytic Paths in H_2 Dissociation on Metal Oxides: The Example of CeO_2. *J. Phys. Chem. C* **2014**, *118*, 10921–10926. [CrossRef]
39. Fernández-Torre, D.; Carrasco, J.; Ganduglia-Pirovano, M.V.; Perez, R. Hydrogen activation, diffusion, and clustering on CeO_2(111): A DFT+U study. *J. Chem. Phys.* **2014**, *141*, 014703. [CrossRef] [PubMed]
40. Wu, Z.; Cheng, Y.; Tao, F.; Daemen, L.; Foo, G.S.; Nguyen, L.; Zhang, X.; Beste, A.; Ramirez-Cuesta, A.J. Direct Neutron Spectroscopy Observation of Cerium Hydride Species on a Cerium Oxide Catalyst. *J. Am. Chem. Soc.* **2017**, *139*, 9721–9727. [CrossRef]
41. Vilé, G.; Dähler, P.; Vecchietti, J.; Baltanás, M.; Collins, S.; Calatayud, M.; Bonivardi, A.; Pérez-Ramírez, J. Promoted ceria catalysts for alkyne semi-hydrogenation. *J. Catal.* **2015**, *324*, 69–78. [CrossRef]
42. Zhou, S.; Gao, L.; Wei, F.; Lin, S.; Guo, H. On the mechanism of alkyne hydrogenation catalyzed by Ga-doped ceria. *J. Catal.* **2019**, *375*, 410–418. [CrossRef]
43. Zhao, Y.; Jalal, A.; Uzun, A. Interplay between Copper Nanoparticle Size and Oxygen Vacancy on Mg-Doped Ceria Controls Partial Hydrogenation Performance and Stability. *ACS Catal.* **2021**, *11*, 8116–8131. [CrossRef]
44. Park, B.Y.; Lim, T.; Han, M.S. A simple and efficient in situ generated copper nanocatalyst for stereoselective semihydrogenation of alkynes. *Chem. Commun.* **2021**, *57*, 6891–6894. [CrossRef] [PubMed]
45. Shi, X.; Lin, Y.; Huang, L.; Sun, Z.; Yang, Y.; Zhou, X.; Vovk, E.; Liu, X.; Huang, X.; Sun, M.; et al. Copper Catalysts in Semihydrogenation of Acetylene: From Single Atoms to Nanoparticles. *ACS Catal.* **2020**, *10*, 3495–3504. [CrossRef]
46. Lu, C.; Wang, Y.; Zhang, R.; Wang, B.; Wang, A. Preparation of an Unsupported Copper-Based Catalyst for Selective Hydrogenation of Acetylene from Cu_2O Nanocubes. *ACS Appl. Mater. Interfaces* **2020**, *12*, 46027–46036. [CrossRef]
47. Zhang, S.; Zhao, C.; Liu, Y.; Li, W.; Wang, J.; Wang, G.; Zhang, Y.; Zhang, H.; Zhao, H. Cu doping in CeO_2 to form multiple oxygen vacancies for dramatically enhanced ambient N_2 reduction performance. *Chem. Commun.* **2019**, *55*, 2952–2955. [CrossRef]
48. Wang, M.; Shen, M.; Jin, X.; Tian, J.; Li, M.; Zhou, Y.; Zhang, L.; Li, Y.; Shi, J. Oxygen Vacancy Generation and Stabilization in CeO_{2-x} by Cu Introduction with Improved CO_2 Photocatalytic Reduction Activity. *ACS Catal.* **2019**, *9*, 4573–4581. [CrossRef]
49. Kresse, G.; Furthmüller, J. Efficient Iterative Schemes for Ab Initio Total-Energy Calculations Using a Plane-wave Basis Set. *Phys. Rev. B* **1996**, *54*, 11169–11186. [CrossRef]
50. Kresse, G.; Furthmüller, J. Efficiency of ab-initio total energy calculations for metals and semiconductors using a plane-wave basis set. *Comput. Mater. Sci.* **1996**, *6*, 15–50. [CrossRef]
51. Perdew, J.P.; Burke, K.; Ernzerhof, M. Generalized gradient approximation made simple. *Phys. Rev. Lett.* **1996**, *77*, 3865. [CrossRef]
52. Blöchl, P.E. Projector augmented-wave method. *Phys. Rev. B* **1994**, *50*, 17953–17979. [CrossRef]
53. Grimme, S.; Antony, J.; Ehrlich, S.; Krieg, H. A consistent and accurate ab initio parametrization of density functional dispersion correction (DFT-D) for the 94 elements H-Pu. *J. Chem. Phys.* **2010**, *132*, 154104. [CrossRef]
54. Krcha, M.D.; Janik, M.J. Challenges in the use of density functional theory to examine catalysis by M-doped ceria surfaces. *Int. J. Quantum Chem.* **2014**, *114*, 8–13. [CrossRef]
55. McFarland, E.W.; Metiu, H. Catalysis by Doped Oxides. *Chem. Rev.* **2013**, *113*, 4391–4427. [CrossRef]
56. Fabris, S.; Vicario, G.; Balducci, G.; de Gironcoli, S.; Baroni, S. Electronic and Atomistic Structures of Clean and Reduced Ceria Surfaces. *J. Phys. Chem. B* **2005**, *109*, 22860–22867. [CrossRef] [PubMed]
57. Henkelman, G.; Uberuaga, B.P.; Jónsson, H. A climbing image nudged elastic band method for finding saddle points and minimum energy paths. *J. Chem. Phys.* **2000**, *113*, 9901–9904. [CrossRef]
58. Wan, Q.; Chen, Y.; Zhou, S.; Lin, J.; Lin, S. Selective hydrogenation of acetylene to ethylene on anatase TiO_2 through first-principles studies. *J. Mater. Chem. A* **2021**, *9*, 14064–14073. [CrossRef]
59. Guo, C.; Wei, S.; Zhou, S.; Zhang, T.; Wang, Z.; Ng, S.-P.; Lu, X.; Wu, C.-M.L.; Guo, W. Initial Reduction of CO_2 on Pd-, Ru-, and Cu-Doped CeO_2(111) Surfaces: Effects of Surface Modification on Catalytic Activity and Selectivity. *ACS Appl. Mater. Interfaces* **2017**, *9*, 26107–26117. [CrossRef]